Received 20 April 2024, accepted 8 May 2024, date of publication 13 May 2024, date of current version 21 May 2024.

Digital Object Identifier 10.1109/ACCESS.2024.3400049

RESEARCH ARTICLE

Design and Implementation of the Luenberger Observer for Estimating the Voltage Response of a PEM Electrolyzer During Supply Current Variations

ÁNGEL HERNÁNDEZ-GÓMEZ[1], DIEGO LANGARICA-CORDOBA[1], (Senior Member, IEEE), PANFILO R. MARTINEZ-RODRIGUEZ[1], (Senior Member, IEEE), HERNÁN GONZÁLEZ-AGUILAR[1], DAMIEN GUILBERT[2], (Member, IEEE), AND BELEM SALDIVAR[3]

[1]School of Sciences, Universidad Autónoma de San Luis Potosí (UASLP), San Luis Potosí 78295, Mexico
[2]GREAH, Université Le Havre Normandie, 76600 Le Havre, France
[3]Department of Automatic Control, CINVESTAV-IPN, Instituto Politécnico Nacional, Mexico City 07360, Mexico

Corresponding author: Belem Saldivar (belem.saldivar@cinvestav.mx)

This work was supported by the Consejo Nacional de Humanidades, Ciencias y Tecnologías (CONAHCYT), Mexico.

ABSTRACT Equivalent electrical circuits (ECM) have proven to be effective in modeling the dynamic behavior of proton exchange membrane (PEM) electrolyzer voltage response. They are a valuable tool for studying the interactions between power electronics and PEM electrolyzers during dynamic operating conditions. Generally, the ECM takes into consideration the activation over-voltage that is present at both the anode and the cathode for the dynamic part of the model. Therefore, the monitoring of the ECM activation over-voltage is an important issue for the correct modeling of the PEM electrolyzer voltage. However, voltage sensors for this over-voltage are expensive and the reported observers of the PEM electrolyzer activation over-voltage are scarce and have not been validated over a sufficiently long time. This work aims at overcoming these drawbacks by proposing the use of a Luenberger observer to accurately estimate the activation over-voltage using an ECM. Based on this proposal, it is possible to build a device capable of emulating the electrolyzer voltage efficiently. Furthermore, a stability analysis of the observable system is provided to ensure its performance throughout the experiment period. Statistical results, based on experimental voltage data from a PEM electrolyzer QL–300, demonstrate the high accuracy and performance of the Luenberger observer under continuous changes in input currents, which demonstrates its robustness.

INDEX TERMS Electronic circuit model, Luenberger observer, PEM electrolyzer, stability analysis, voltage behavior.

I. INTRODUCTION

Electrolyzers have demonstrated their importance in the production of green hydrogen from environmentally friendly power sources, which is considered one of the main fuels to meet the energy demand of the coming years [1], [2]. The basic operation of an electrolyzer is the production of highly pure hydrogen through the process of water electrolysis [3]. Despite the different technologies developed and reported in the literature for electrolyzers (i.e., solid oxide, anion exchange membrane, alkaline and proton exchange membrane (PEM)), only alkaline and PEM electrolyzers have reached the commercial stage. Between these two technologies, PEM electrolyzers have evidenced to have a better response when coupled with renewable energies due to their operational flexibility [4].

The associate editor coordinating the review of this manuscript and approving it for publication was Fangfei Li.

Mathematical modeling of the PEM electrolyzer that efficiently describes the behavior of its internal and external processes, has largely contributed to the development of the PEM electrolyzer technology. Furthermore, with these mathematical models, it is possible to design controllers, failure analysis, energy management, and optimization of the PEM electrolyzer system [5], [6], [7], [8], [9]. Mathematical models of PEM electrolyzers are classified as analytical, empirical, and mechanistic. Commonly, analytical models consider the performance of the electrolyzer to determine the behavior of the main variables that influence it. Empirical models use experimental data to determine system parameters. However, a disadvantage of these models is that they are limited to a specific PEM electrolyzer. Mechanistic models are more complex compared to the other two types of modeling since they use differential or algebraic equations to perform highly reliable simulations of the phenomena that occur in the electrolyzer. It is worth mentioning that the time to perform the simulations of the mechanistic models is considerable due to the extensive calculations [10].

Dynamic models, which belong to the class of mechanistic models, are useful to describe systems in real-time, besides, from these models, control theory can be applied [11]. The equivalent electronic circuit model (ECM), which belongs to the dynamic models, allows modeling the PEM electrolyzer voltage response during dynamic operating conditions [12]. Usually, the ECM takes into account the over-voltages that occur within the PEM electrolyzer [13], [14]. Furthermore, these over-voltages can be classified as ohmic, activation, and concentration [15]. In particular, the voltage responses of the PEM electrolyzer take place in the activation over-voltage [16]. Therefore, to efficiently reproduce the voltage of a PEM electrolyzer (to build a voltage emulator based on an ECM), it is important to be able to observe the dynamic behavior of the activation over-voltage [17]. To carry out this task, voltage sensors can be used, which are usually expensive depending on the measurement accuracy. Also, it is possible to replace the measurements of the voltage sensors with the estimations of an observer, which only depend on the input and output signals [18]. Different types of observers have been applied to different research fields, such as PEM fuel cells [19], [20], batteries [21], and underactuated quadrotors [22], [23]. Table 1 shows examples of observers recently applied to different research fields and their details. However, observers for the PEM electrolyzer activation over-voltage are scarce and have not been implemented during a long enough time window [24]. For this reason, the development of observers for PEM electrolyzers is important for the study of responses to dynamic oscillations in the voltage.

Due to the importance of observers for the PEM electrolyzer voltage, this work aims at implementing the Luenberger observer in an ECM since this observer has proven to be practical and robust for linear observable systems [32]. As mentioned in [33], for less complex linear systems, the Luenberger observer is the best choice among other techniques such as Bayesian estimators or AI-based observers, as it provides a valid estimate of the system state without requiring complex computational methods that are usually time-consuming or difficult to implement.

TABLE 1. Examples of observers applied to research fields.

Reference	Observer	Field	Application
[21]	Nonlinear	Batteries	Active species concentrations
[22]	Extended state	Underactuated quadrotor	Helical trajectory tracking
[23]	Luenberger	Underactuated quadrotor	Helical trajectory tracking
[24]	Luenberger	PEM electrolyzer	Activation over-voltage
[25]	Nonlinear Distributed Parameters	PEM fuel cell	Internal states
[26]	Extended state	PEM fuel cell	Oxygen excess ratio
[27]	Kalman filter	Batteries	state of charge
[28]	Multi-objective nonlinear	Batteries	Fault detection
[29]	Bayesian	Natural daylight	Hue perception
[30]	Impulsive	Wind energy	Flux detection
[31]	Event-triggered impulsive	Disturbed states and disturbed outputs	State of DC micrograds
The present paper	Luenberger	PEM electrolyzer	Activation over-voltage

The main characteristics and contributions of the proposed observer in this work are presented below.

- The observability and stability of the system were demonstrated to ensure the effectiveness of the observer throughout the experimental test (4000 s).
- A comparison of the observer with experimental data under constant disturbances in the input current (square wave function at different periods using dSPACE controller board) from a PEM electrolyzer QL–300 of Shandong Saikesaisi Hydrogen Energy Co was made. This comparison validated the performance and robustness of the observer of the activation voltage (i.e., statistical tests were applied).
- It is possible to build a device that efficiently emulates the PEM electrolyzer voltage by implementing the proposed observer with the ECM design of this work.

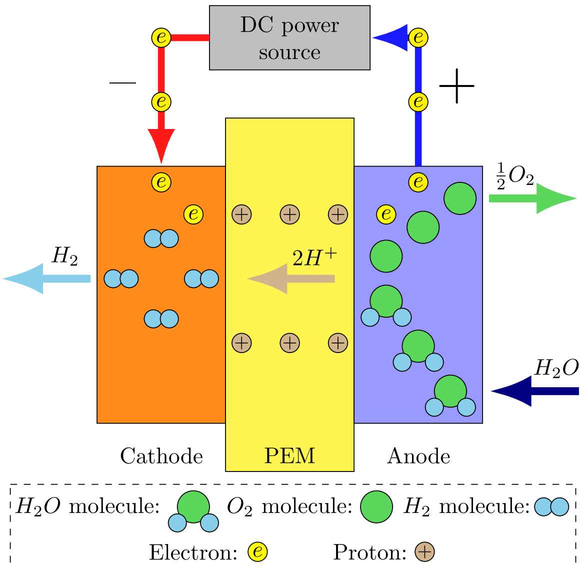

FIGURE 1. PEM electrolyzer basic operation.

The rest of the work is structured as follows: after discussing the state-of-the-art and motivations in the introduction, Section II presents a detailed description of the experimental platform. In Section III, the description of an ECM for estimating the PEM electrolyzer voltage is shown. Besides, in this section, the design of the Luenberger observer and the stability analysis of the observable system are provided. Subsequently, in Section IV, the simulations of the estimations from the observer and the discussion of this work are shown. Finally, in Section V, the conclusion is presented.

II. EXPERIMENTAL TEST SET-UP

A. PEM ELECTROLYZER BASIC OPERATION

To carry out electrolysis, the PEM electrolyzer generally operates with an anode, a cathode, a PEM (usually Nafion), and a DC power source. Each part of the PEM electrolyzer system serves a fundamental purpose: at the anode, oxygen, electrons, and protons are produced; the produced protons pass to the cathode through the PEM; the external circuit connected to the DC power source flows the electrons from the anode to the cathode; hydrogen is produced at the cathode by combining protons with electrons [34], [35], see Figure 1. The reactions in the PEM electrolyzer are presented in (1).

$$H_2O \rightarrow 2H^+ + \frac{1}{2}O_2 + 2e^- \text{ (Anode reaction)}$$
$$2H^+ + 2e^- \rightarrow H_2 \text{ (Cathode reaction)}$$
$$H_2O \rightarrow H_2 + \frac{1}{2}O_2 \text{ (General reaction)} \quad (1)$$

The PEM electrolyzer is a promising technology despite being less efficient than the alkaline electrolyzer due to its wide operating range, high current densities ($2\,A \cdot cm^{-2}$), fast response time, and good performance when combined with renewable energy sources. Therefore, the PEM electrolyzer can cope with fluctuations from intermittent energy sources due to its partial load [36], [37].

TABLE 2. PEM electrolyzer QL–300 specifications.

Parameter	Value	Unit
Hydrogen purity	≥99.999	%
Hydrogen output flow range	0–310.3	$mL \cdot min^{-1}$
Output pressure range	0.2–4	*bar*
Pressure stability	<0.01	*bar*
Electrical power range	0–150	*W*
Operating voltage range	1.4–2.5	*V*
Current range	0–60	*A*
Cell number	1	–
Active area section	150	cm^2
Solid Polymer Electrolyte (SPE)	183	μm

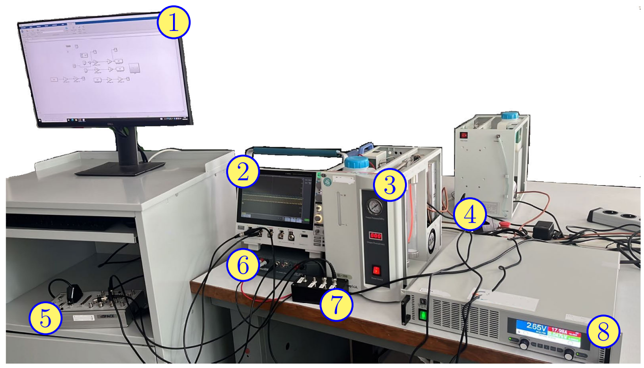

FIGURE 2. Equipment and experimental test set-up.

B. EXPERIMENTAL DATABASE COLLECTION

The different databases were obtained from the PEM electrolyzer QL–300 of Shandong Saikesaisi Hydrogen Energy Co., Ltd. (Jinan, China). The characteristics of this electrolyzer are shown in Table 2.

To obtain reliable databases, the equipment and experimental test described below were proposed, see Figure 2.

(1) A computer with Matlab-Simulink ®.
(2) An oscilloscope MDO34–1000 of Tektronix Company.
(3) A PEM electrolyzer QL–300.
(4) An electrical current sensor.
(5) A DS1104 controller board from dSPACE Company.
(6) A voltage sensor.
(7) A signal converter from the dSPACE control to the DC power supply.
(8) A DC power supply EL 9160–100 of Elektro Automatick (EA) Company.

Seven databases were taken, each data collection had a duration of 4000 seconds and the following mechanics were carried out: A square wave current signal was programmed in Matlab-Simulink ® for the dSPACE controller board (i.e., minimum and maximum current values, see Table 4); the dSPACE controller sent this signal to the DC power source using a signal converter; the PEM electrolyzer was supplied by the DC power source using a square wave current signal;

TABLE 3. ECM and Luenberger observer parameters.

Parameter	Description	Unit
C_a	Equivalent capacitor (anode)	F
C_c	Equivalent capacitor (cathode)	F
e	Estimation error	V
i_{el}	PEM electrolyzer current	A
L	Luenberger gains vector	—
R_a	Equivalent resistor (anode)	Ω
R_c	Equivalent resistor (cathode)	Ω
R_{mem}	Membrane resistor	Ω
u	System input	A
v_{act}	Activation over-voltage	V
$v_{act,a}$	Activation over-voltage (anode)	V
$v_{act,c}$	Activation over-voltage (cathode)	V
v_{con}	Concentration over-voltage	V
v_e	PEM electrolyzer voltage	V
v_{ini}	DC voltage source	V
v_{rev}	Reversible over-voltage	V
v_Ω	Ohmic over-voltage	V
x	System states	V
x_0	Initial condition of states	V
$\hat{x}$	System estimated states	V
y	System output	V
τ_a	Electrical time constant (anode)	s
τ_c	Electrical time constant (cathode)	s

the database of the voltage and current sensors was projected and saved by the oscilloscope.

Figure 3 shows the experimental results obtained for the PEM electrolyzer voltage databases and their respective square waveform input currents. The different square waveform current inputs were generated through Matlab–Simulink® and dSPACE in a minimum step range of 0 to 10 A and a maximum step range of 7 to 20 A with switching periods of 25 seconds (Figure 3.a), 50 seconds (Figure 3.b), and 100 seconds (Figure 3.c). The different voltage responses varied between 1.6 and 2.2 V for the minimum current input steps and varied between 1.9 and 2.4 V for the maximum current input steps. It is worth mentioning that the PEM electrolyzer voltage is usually variable due to different factors that occur in the electrolyzer such as pressure, temperature, and the power source (renewable energy source). After obtaining the experimental databases, the Luenberger observer was developed and implemented for an ECM in Section III.

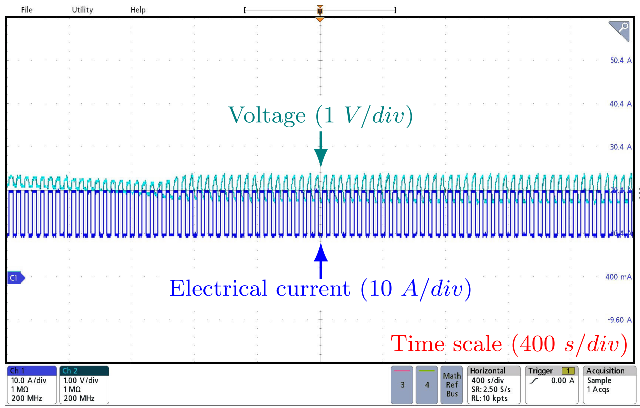

(a) Period of 25 seconds.

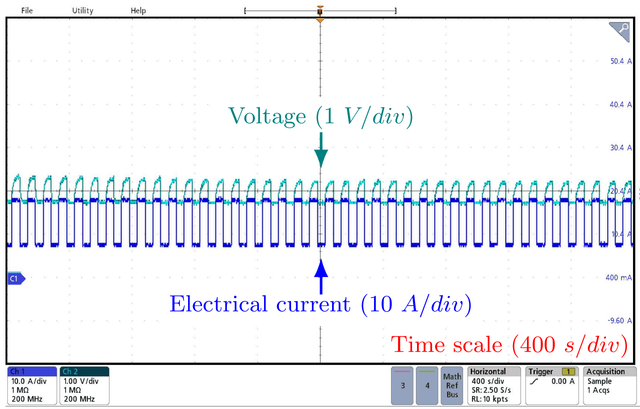

(b) Period of 50 seconds.

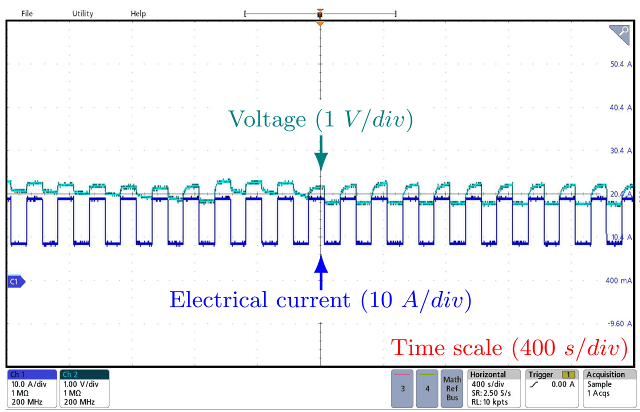

(c) Period of 100 seconds.

FIGURE 3. PEM electrolyzer voltage behavior with different input square waveform currents.

III. DESIGN OF THE LUENBERGER OBSERVER FOR THE PEM ELECTROLYZER VOLTAGE

To start this section, the description of the parameters used in the ECM and observer equations are shown in Table 3.

A. PEM ELECTROLYZER MATHEMATICAL MODEL

In this work, the ECM developed in [38] and [39] is used. The PEM electrolyzer voltage v_e is expressed in terms of the reversible v_{rev}, ohmic v_Ω, activation v_{act}, and concentration v_{con} over-voltages as follows:

$$v_e = v_{rev} + v_\Omega + v_{act} + v_{con}. \tag{2}$$

The ECM for (2) is defined as follows:

- A constant DC voltage source v_{ini} is used for modeling v_{rev},

$$v_{rev} = v_{ini}. \tag{3}$$

- A constant resistance is used for modeling the electrolyzer membrane R_{mem}, thus v_Ω is expressed as:

$$v_\Omega = R_{mem} i_{el}, \tag{4}$$

where i_{el} is the PEM electrolyzer current (A).

- Two resistor-capacitor branches are used for modeling v_{act}, one for the cathode $v_{act,c}$ and the other for the

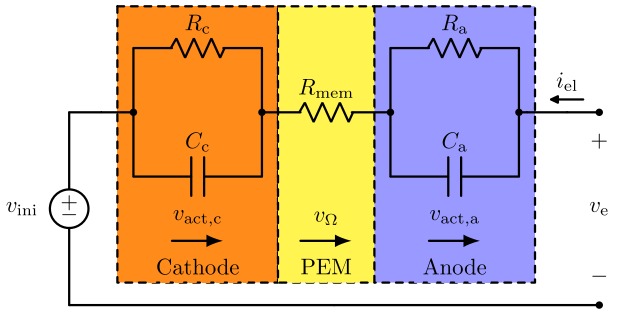

FIGURE 4. Equivalent electronic circuit diagram for PEM electrolyzer voltage.

anode $v_{act,a}$. Besides, it has been reported that the PEM electrolyzer voltage dynamic occurs at this over-voltage.

$$v_{act} = v_{act,c} + v_{act,a}, \tag{5}$$

where the dynamic equations are defined as:

$$\frac{dv_{act,c}}{dt} = \frac{1}{C_c} i_{el} - \frac{1}{\tau_c} v_{act,c}, \tag{6}$$
$$\frac{dv_{act,a}}{dt} = \frac{1}{C_a} i_{el} - \frac{1}{\tau_a} v_{act,a}, \tag{7}$$

where C_c and C_a are the equivalent capacitors for the cathode and the anode in (F), respectively. τ_c and τ_a are the electrical time constants that depend strongly on the operating conditions at the cathode and the anode in (s), respectively. R_c and R_a are the resistors for the cathode and the anode in (Ω), respectively. Besides, R_c and R_a are calculated using τ_c and τ_a as follows:

$$\tau_c = C_c R_c, \tag{8}$$
$$\tau_a = C_a R_a. \tag{9}$$

- Finally, v_{con} is estimated as zero because this over-voltage has been reported to be considerably smaller than v_{act} and v_Ω [40], [41].

So, the ECM for the PEM electrolyzer voltage is expressed as:

$$v_e(t) = v_{ini} + R_{mem} i_{el}(t) + v_{act}(t). \tag{10}$$

Figure 4 shows the equivalent electronic circuit diagram for PEM electrolyzer voltage using the electronic components that make up the ECM (i.e., one DC voltage source, two capacitors, and three resistors). Therefore, this diagram is useful for constructing a real equivalent electronic circuit to emulate the PEM electrolyzer voltage.

B. DEVELOPMENT OF THE LUENBERGER OBSERVER

In this subsection, the equations describing the PEM electrolyzer voltage are defined as a control system, so that it is easier to structure the Luenberger observer. So, let y be defined as follows:

$$y := v_e - v_{ini}, \tag{11}$$

and

$$\begin{aligned} x_1 &:= v_{act,c}, \\ x_2 &:= v_{act,a}, \\ u &:= i_{el}. \end{aligned} \tag{12}$$

Substituting (11) and (12) in (6), (7), and (10), it is obtained:

$$\dot{x}_1 = \frac{1}{C_c} u - \frac{1}{\tau_c} x_1, \tag{13}$$
$$\dot{x}_2 = \frac{1}{C_a} u - \frac{1}{\tau_a} x_2, \tag{14}$$
$$y = R_{mem} u + x_1 + x_2. \tag{15}$$

where $x = [x_1, x_2]^T$ with initial condition $x_0 = [x_{1,0}, x_{2,0}]^T$. Then, the system can be represented as:

$$\dot{x} = Ax + Bu, \tag{16}$$

where

$$A = \begin{pmatrix} A_{11} & 0 \\ 0 & A_{22} \end{pmatrix} = \begin{pmatrix} -\frac{1}{\tau_c} & 0 \\ 0 & -\frac{1}{\tau_a} \end{pmatrix} \tag{17}$$

and

$$B = \begin{pmatrix} B_1 \\ B_2 \end{pmatrix} = \begin{pmatrix} \frac{1}{C_c} \\ \frac{1}{C_a} \end{pmatrix} \tag{18}$$

And let

$$y = Cx + Du \tag{19}$$

where $C = [1, 1]$ and $D = R_{mem}$.

To implement the Luenberger observer to the system defined in (16)–(19), it is necessary to prove that this system is observable. Therefore, the rank of the observability matrix defined below was calculated for $A_{11} \neq A_{22}$ and $\forall s \in \mathbb{C}$,

$$\text{rank}\begin{bmatrix} sI - A \\ C \end{bmatrix} = \text{rank}\begin{bmatrix} s - A_{11} & 0 \\ 0 & s - A_{22} \\ 1 & 1 \end{bmatrix} = 2. \tag{20}$$

By applying the observability matrix criterion [42], one can conclude that the system is observable.

Once the observability property of the system is demonstrated, the Luenberger observer is constructed. This observer is built with the original system including the estimation error to compensate for the inaccuracies in A and B [43]. In this way, the observer model is defined as:

$$\begin{aligned} \dot{\hat{x}} &= A\hat{x} + Bu + L(y - C\hat{x} - Du) \\ &= (A - LC)\hat{x} + (B - LD)u + Ly, \end{aligned} \tag{21}$$

where $\hat{x} = [\hat{x}_1, \hat{x}_2]^T$ is the estimated state and, therefore, $C\hat{x} + Du$ is the estimated output. $L = [l_1, l_2]^T$ is the Luenberger vector, which is a weighting vector that continuously corrects the model output and improves the observer's behavior. The error vector e is defined as the difference between x and $\hat{x}$:

$$e := x - \hat{x}. \tag{22}$$

Therefore, the dynamic of vector e is given by:

$$\begin{aligned}\dot{e} &= \dot{x} - \dot{\hat{x}} \\ &= (A - LC)(x - \hat{x}) \\ &= (A - LC)e. \end{aligned} \tag{23}$$

Therefore, the eigenvalues of the matrix $(A - LC)$ must be negative to ensure that e converges to zero and that x converges to $\hat{x}$ exponentially. Thus, this work proposes conditions on L for which the matrix $(A - LC)$ has negative eigenvalues. Consider the following expression to calculate the eigenvalues λ:

$$\det(\lambda I - A + LC) = 0. \tag{24}$$

The following expression is obtained from (24):

$$\lambda^2 + b\lambda + c = 0. \tag{25}$$

where $b = l_1 + l_2 - A_{11} - A_{22}$ and $c = A_{11}A_{22} - A_{11}l_2 - A_{22}l_1$ Therefore, the eigenvalues of the matrix are given by:

$$\lambda = \frac{-b \pm \sqrt{b^2 - 4c}}{2}, \tag{26}$$

To find conditions for which the eigenvalues are negative, note that the discriminant satisfies:

$$\begin{aligned} b^2 - 4c &= (A_{22} - A_{11})^2 + 2(A_{22} - A_{11})(l_1 - l_2) \\ &\quad + (l_1 + l_2)^2 \\ &= [(A_{22} - A_{11}) + (l_1 - l_2)]^2 + (l_1 + l_2)^2 \\ &\quad - (l_1 - l_2)^2 \\ &= [(A_{22} - A_{11}) + (l_1 - l_2)]^2 + 4l_1 l_2. \end{aligned}$$

Given the above developments, $(b^2 - 4c)$ is positive as long as l_1 and l_2 have the same sign or if $l_1 + l_2 > |l_1 - l_2|$. Now, suppose both values of L are greater or equal to zero $l_1, l_2 \geq 0$ (the case when $l_1 = l_2 = 0$ is the original system (16), which is nominally stable). Then, as the values of $-A_{11} = \frac{1}{\tau_c}$ and $-A_{22} = \frac{1}{\tau_a}$ are greater than zero by hypothesis, it is obtained that $b > 0$ and $c > 0$. Therefore,

$$\lambda_1 = \frac{-b - \sqrt{b^2 - 4c}}{2} < 0.$$

Besides, it holds that $\sqrt{b^2 - 4c} < \sqrt{b^2} = |b| = b$. Thus, $-b + \sqrt{b^2 - 4c} < 0$ and hence

$$\lambda_2 = \frac{-b + \sqrt{b^2 - 4c}}{2} < 0.$$

Therefore, the system (23) is stable when $l_1, l_2 \geq 0$. For the cases when $l_1, l_2 \leq 0$ and $l_1 + l_2 > |l_1 - l_2|$ the restrictions that guarantee negative eigenvalues for (23) are derived below.

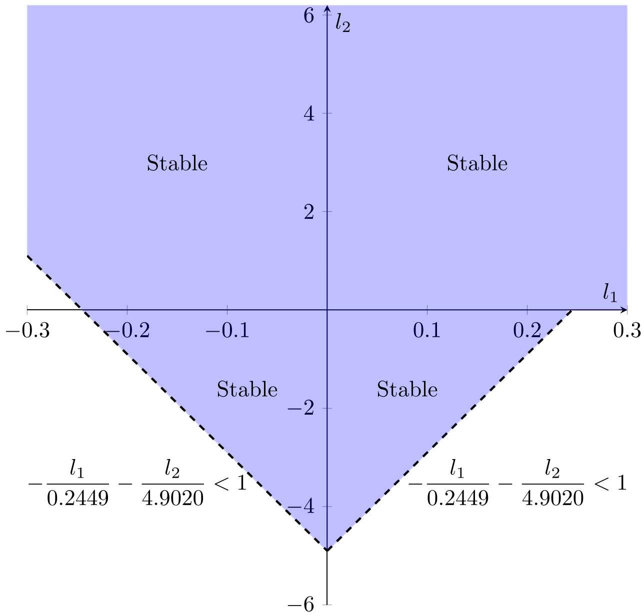

FIGURE 5. Demonstrated stable region for the system (23) using $\tau_c = 4.0835$ and $\tau_a = 0.2040$.

It is worth mentioning that case $l_1 + l_2 > |l_1 - l_2|$ involves the following two cases:

Case 1	Case 2
$l_1 + l_2 > l_1 - l_2$	$l_1 - l_2 > -l_1 - l_2$
$l_2 > -l_2$	$l_1 > -l_1$
$2 \cdot l_2 > 0$	$2 \cdot l_1 > 0$
$l_2 > 0$	$l_1 > 0.$

Now, to ensure that $b > 0$, let $l_1 + l_2 > A_{11} + A_{22}$, so that, for the cases when $l_1, l_2 \leq 0$ and $l_1 + l_2 > |l_1 - l_2|$, $b > 0$. Therefore, $\lambda_1 < 0$. Furthermore, to guarantee that $c > 0$, it is assumed that l_1 and l_2 satisfy $\frac{l_1}{A_{11}} + \frac{l_2}{A_{22}} < 1$. Thus, it is obtained that $A_{11}l_2 + A_{22}l_1 < A_{11}A_{22}$. Consequently, $c > 0$, and taking into consideration that $b > 0$, it holds that $\sqrt{b^2 - 4c} < \sqrt{b^2} = |b| = b$. Thus, $\lambda_2 < 0$.

Therefore, for the cases when $l_1, l_2 \leq 0$ and $l_1 + l_2 > |l_1 - l_2|$, the system (23) is stable if $l_1 + l_2 > A_{11} + A_{22}$, and $\frac{l_1}{A_{11}} + \frac{l_2}{A_{22}} < 1$. Figure 5 illustrates the demonstrated stable region of the system (23) for $\tau_c = 4.0835$ and $\tau_a = 0.2040$ (these values were considered according to [38]).

Once the observer was determined and its stability region demonstrated, it was simulated. The simulation results of the proposed observer are shown in the next section.

IV. RESULTS AND DISCUSSION

In this section, the simulation results of the observer response are presented in detail. Besides, a discussion of the outcomes is presented.

TABLE 4. Maximum and minimum input current i_{el} and values τ_c and τ_a for each database.

Database	i_{el}	τ_{c}	τ_{a}
Database 1	min $= 10\,A$, max $= 20\,A$	$4.0835\ s$	$0.2040\ s$
Database 2	min $= 1\,A$, max $= 20\,A$	$3.4917\ s$	$0.4819\ s$
Database 3	min $= 5\,A$, max $= 15\,A$	$4.0336\ s$	$0.6644\ s$
Database 4	min $= 6\,A$, max $= 16\,A$	$3.9747\ s$	$0.6556\ s$
Database 5	min $= 8\,A$, max $= 18\,A$	$3.9822\ s$	$0.4040\ s$
Database 6	min $= 9\,A$, max $= 19\,A$	$3.7851\ s$	$0.4321\ s$
Database 7	min $= 2\,A$, max $= 7\,A$	$4.6681\ s$	$1.5860\ s$

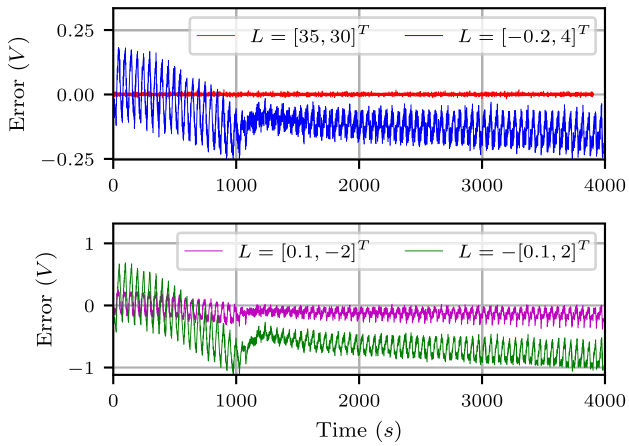

FIGURE 6. Observer error behavior with different values of L (stable region) for database 1.

A. SIMULATION AND VALIDATION

To carry out the simulations, the Python programming language was used (Python version: 3.8.10 for 64 bits, processor: Intel CORE i7-7700 HQ CPU, 2.80 GHz, operating system: Windows 10). The proposed observer was simulated using the parameter values $v_{\text{ini}} = 1.43\ V$, $R_{\text{mem}} = 0.0155\ \Omega$, and $C_{\text{c}} = C_{\text{a}} = 125\ F$. Furthermore, as mentioned in [39], the parameters τ_c and τ_a are constants that depend on the input current and other relevant parameters (gas pressure and temperature that are not considered in this current work), for this reason, different values for these parameters were used depending on the database, see Table 4.

The behavior of the observer error under different values of L (l_1 and l_2 at different points of the stability region) was analyzed using Databases 1 and 2. For Database 1, the Luenberger observer obtained better performance when using $l_1, l_2 > 0$ with a relative error of 0.075%, while in the other cases $l_1 < 0$ and $l_2 > 0$, $l_1 > 0$ and $l_2 < 0$, and $l_1, l_2 < 0$ obtained a relative errors of 3.3717%, 3.6469%, and 17.5394%, respectively. Figure 6 shows the evolution of the observer error concerning time for Database 1 and different values of L. Similarly, for Database 2, the Luenberger observer obtained a relative error of 0.0911% when using $l_1, l_2 > 0$, which demonstrates the effectiveness of convergence with positive values l_1 and l_2. For the other different values of $l_1 < 0$ and $l_2 > 0$, $l_1 > 0$ and $l_2 < 0$, and $l_1, l_2 < 0$ obtained a relative errors of 1.1219%, 3.0287%, and 4.3968%, respectively. These relative errors obtained

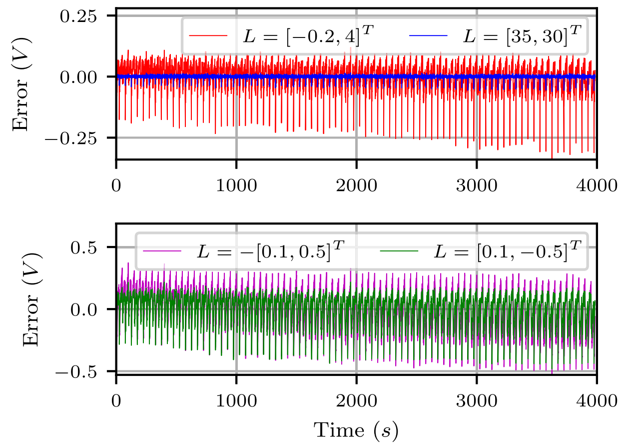

FIGURE 7. Observer error behavior with different values of L (stable region) for database 2.

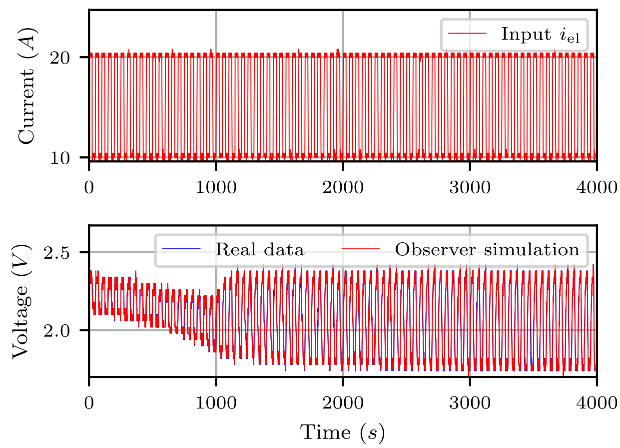

FIGURE 8. Comparison of the observer and Database 1 with its respective input current i_{el}.

from Database 2 are lower compared to those obtained from Database 1 due to the different behavior of the databases. Figure 7 shows the evolution of the observer error concerning time for Database 2 and different values of L. Due to the fast convergence of the error to zero when $l_1, l_2 > 0$, the simulations were developed by considering $l_1 = 35$ and $l_2 = 30$. It is worth mentioning that the higher the values of l_1 and l_2, the faster the convergence. However, computational work is more demanding due to the small step size to achieve solution iterations. For these values of L, the computational operation time for all databases varied between 3.41 and 3.95 seconds. Figure 8 shows the result of the comparison of the observer and Database 1 with its respective input current i_{el} (the dSPACE signal was programmed for an input current of min $= 10\,A$ and max $= 20\,A$).

Figure 9 shows the observed states $v_{\text{act,c}}$ and $v_{\text{act,a}}$ with initial values $v_{\text{act,c,0}} = 0.55\ V$ and $v_{\text{act,a,0}} = 0.03\ V$. In this case, a different behavior can be seen during the first 1000 seconds, which agrees with the voltage shown in Figure 8.

Figure 10 shows the behavior of the observer for Database 2 with its respective input current i_{el} (the dSPACE signal

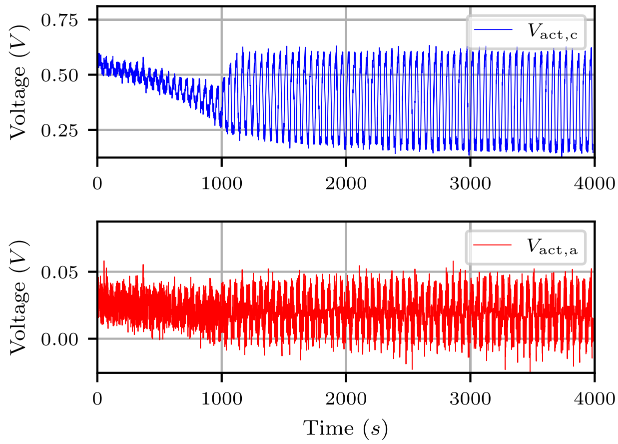

FIGURE 9. Observed states $v_{\text{act,c}}$ and $v_{\text{act,a}}$ for database 1.

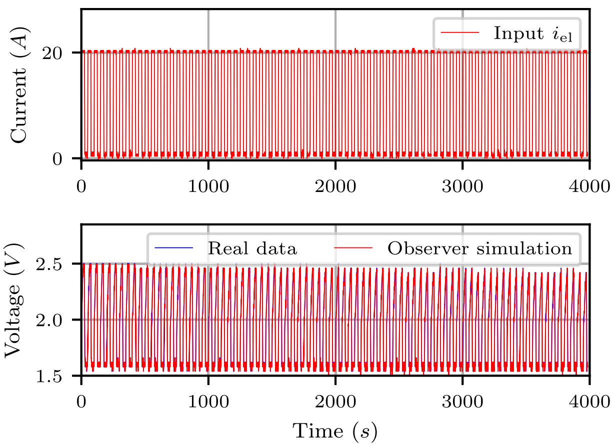

FIGURE 10. Comparison of the observer and Database 2 with its respective input current i_{el}.

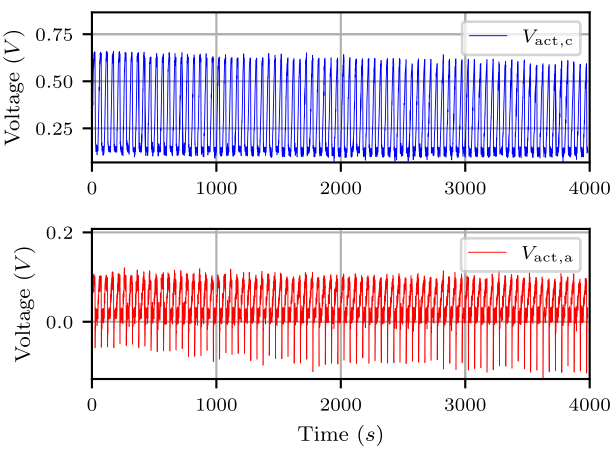

FIGURE 11. Observed states $v_{\text{act,c}}$ and $v_{\text{act,a}}$ for database 2.

was programmed for an input current of min $= 1\ A$ and max $= 20\ A$).

Figure 11 shows the observed states $v_{\text{act,c}}$ and $v_{\text{act,a}}$ with initial values $v_{\text{act,c,0}} = 0.25\ V$ and $v_{\text{act,a,0}} = 0.06\ V$. In this case, a regular voltage behavior can be seen during the experiment, which agrees with the voltage shown in Figure 10.

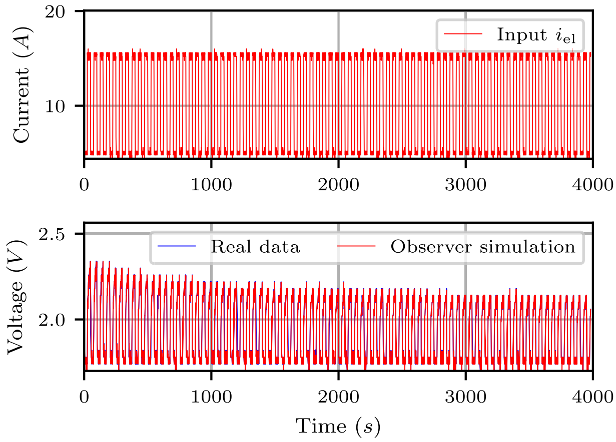

FIGURE 12. Comparison of the observer and database 3 with its respective input current i_{el}.

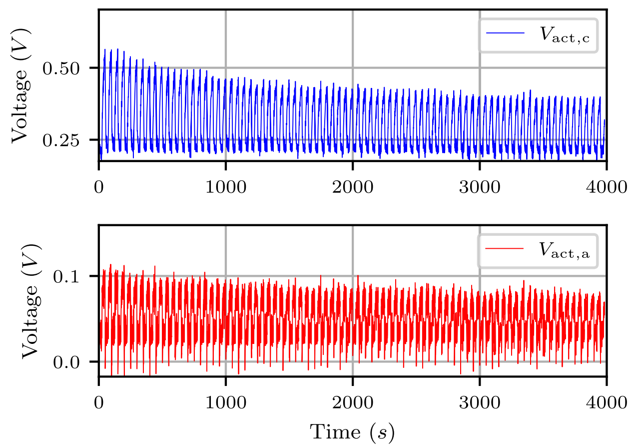

FIGURE 13. Observed states $v_{\text{act,c}}$ and $v_{\text{act,a}}$ for database 3.

Figure 12 shows the input current i_{el} (the dSPACE signal was programmed for an input current of min $=$ $5\ A$ and max $= 15\ A$) and the experimental voltage from Database 3 with its respective estimation using the Luenberger observer. Figure 13 shows the observed states $v_{\text{act,c}}$ and $v_{\text{act,a}}$ with initial values $v_{\text{act,c,0}} = 0.29\ V$ and $v_{\text{act,a,0}} = 0.04\ V$. In addition to the high precision observed in Figure 12 between the estimated voltage and the real PEM electrolyzer voltage, the behavior of the observed states agrees with the system output, which proves the effectiveness of the proposed observer.

Figure 14 shows the result of the comparison of the observer and Database 4 with its respective input current i_{el} (the dSPACE signal was programmed for an input current of min $= 6\ A$ and max $= 16\ A$).

Figure 15 shows the observed states $v_{\text{act,c}}$ and $v_{\text{act,a}}$ with initial values $v_{\text{act,c,0}} = 0.52\ V$ and $v_{\text{act,a,0}} = 0.08\ V$. In this case, a different behavior is observed around the first 1400 seconds, which agrees with the voltage shown in Figure 14.

Figure 16 shows the behavior of the observer for Database 5 with its respective input current i_{el} (the dSPACE signal was

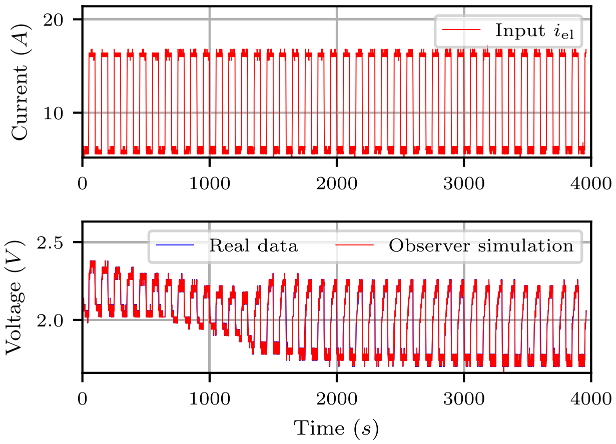

FIGURE 14. **Comparison of the observer and Database 4 with its respective input current i_{el}.**

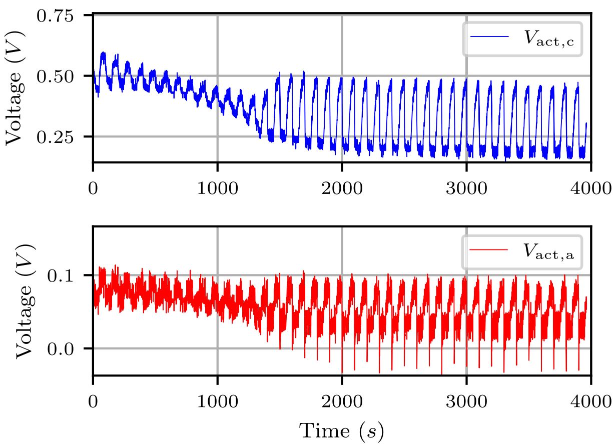

FIGURE 15. **Observed states $v_{act,c}$ and $v_{act,a}$ for database 4.**

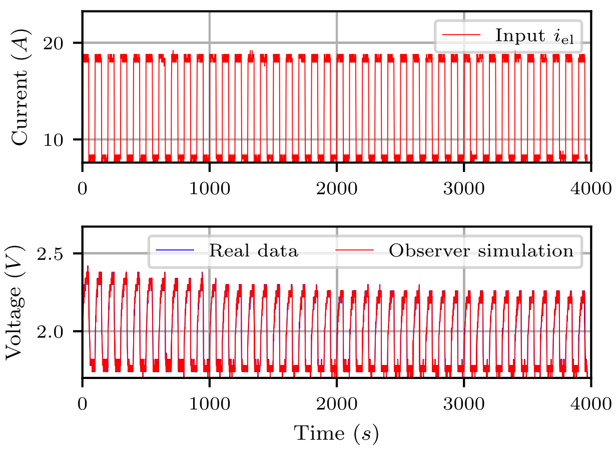

FIGURE 16. **Comparison of the observer and database 5 with its respective input current i_{el}.**

programmed for an input current of min $= 8\,A$ and max $= 18\,A$).

Figure 17 shows the observed states $v_{act,c}$ and $v_{act,a}$ with initial values $v_{act,c,0} = 0.27\ V$ and $v_{act,a,0} = 0.05\ V$. The effectiveness of the observer is demonstrated by the high precision between the estimated voltage and the real voltage

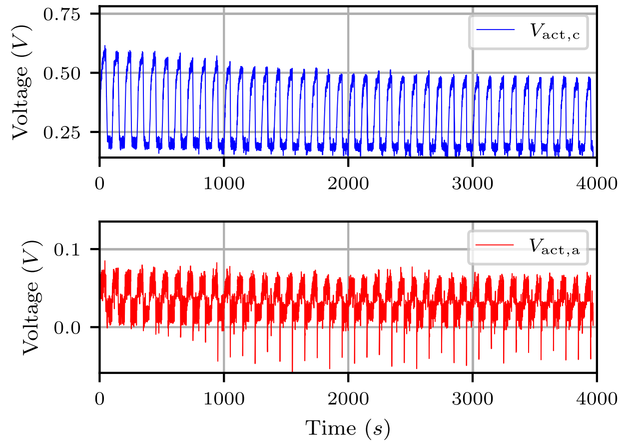

FIGURE 17. **Observed states $v_{act,c}$ and $v_{act,a}$ for database 5.**

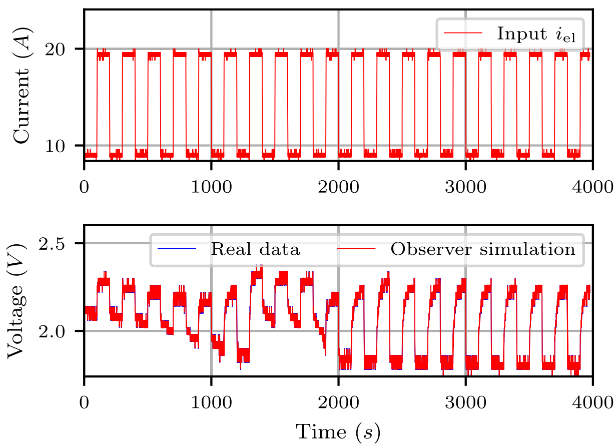

FIGURE 18. **Comparison of the observer and Database 6 with its respective input current i_{el}.**

of the PEM electrolyzer shown in Figure 16 and the behavior of the observed states, which agrees with the output of the system.

Figure 18 shows the input current i_{el} (the dSPACE signal was programmed for an input current of min $= 9\ A$ and max $= 19\ A$) and the experimental voltage from Database 6 with its respective estimation using the Luenberger observer.

Figure 19 shows the observed states $v_{act,c}$ and $v_{act,a}$ with initial values $v_{act,c,0} = 0.52\ V$ and $v_{act,a,0} = 0.05\ V$. This Database showed the most irregular behavior of all the databases. However, as can be seen in Figures 18 and 19, the high accuracy of the simulated voltage in estimating the real voltage and the behavior of the observed states demonstrate that the proposed observer is efficient and robust. Figure 20 shows the result of the comparison of the observer and Database 7 with its respective input current i_{el} (the dSPACE signal was programmed for an input current of min $= 2\ A$ and max $= 7\ A$). Figure 21 shows the observed states $v_{act,c}$ and $v_{act,a}$ with initial values $v_{act,c,0} = 0.22\ V$ and $v_{act,a,0} = 0.03\ V$. In this case, a regular behavior can be seen during the experiment, which agrees with the voltage shown in Figure 21.

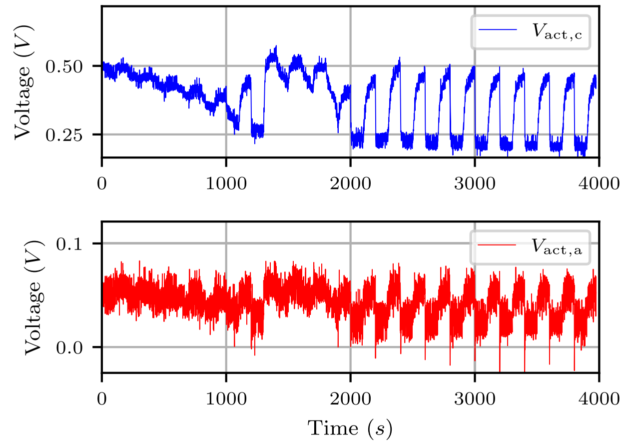

FIGURE 19. Observed states $v_{act,c}$ and $v_{act,a}$ for Database 6.

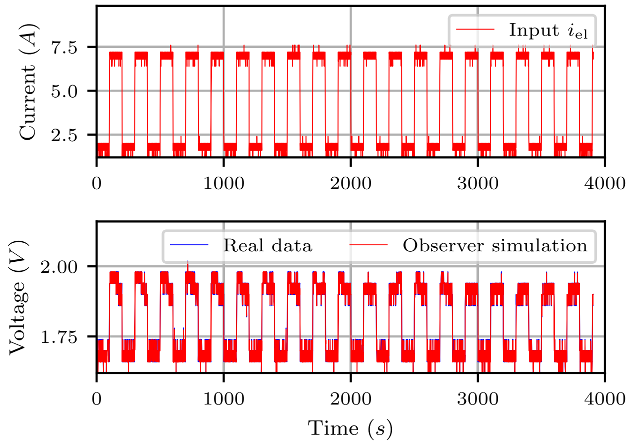

FIGURE 20. Comparison of the observer and database 7 with its respective input current i_{el}.

Statistical tests were applied after observing the comparisons of the different databases with the Luenberger observer. The results of these tests are shown in the next subsection.

B. DISCUSSION

Relative error $E_{\rm r}$, mean error $E_{\rm m}$, mean squared error MSE, and root mean squared error $RMSE$ were applied to validate the effectiveness of the observer. These statistical tests are given by:

$$E_{\rm r} = \left(\frac{100}{N_d}\right)\sum_{k=1}^{N_d}\left|\frac{v_{{\rm exp},k} - v_{{\rm sim},k}}{v_{{\rm exp},k}}\right|, \tag{27}$$

$$E_{\rm m} = \left(\frac{1}{N_d}\right)\sum_{k=1}^{N_d}\left|v_{{\rm exp},k} - v_{{\rm sim},k}\right|, \tag{28}$$

$$MSE = \left(\frac{1}{N_d}\right)\sum_{k=1}^{N_d}\left(v_{{\rm exp},k} - v_{{\rm sim},k}\right)^2, \tag{29}$$

$$RMSE = \sqrt{MSE}, \tag{30}$$

where N_d is the number of voltage data (i.e., N_d varied between 9904 and 9970). $v_{{\rm exp},k}$ is the k-th voltage data measurement and $v_{{\rm sim},k}$ is the k-th voltage data simulation. The statistical test results are shown in Table 5.

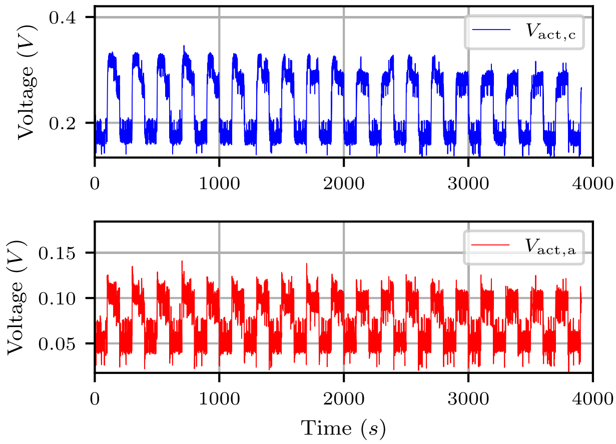

FIGURE 21. Observed states $v_{act,c}$ and $v_{act,a}$ for database 7.

TABLE 5. Statistical test results.

Database	$E_{\rm r}$	$E_{\rm m}$	MSE	$RMSE$
Database 1	0.0750%	0.0027 V	1.25e^{-5} V^2	0.0035 V
Database 2	0.0911%	0.0030 V	2.78e^{-5} V^2	0.0053 V
Database 3	0.0752%	0.0025 V	1.20e^{-5} V^2	0.0035 V
Database 4	0.0746%	0.0025 V	1.16e^{-5} V^2	0.0034 V
Database 5	0.0773%	0.0026 V	1.29e^{-5} V^2	0.0036 V
Database 6	0.0768%	0.0027 V	1.20e^{-5} V^2	0.0035 V
Database 7	0.0771%	0.0025 V	1.13e^{-5} V^2	0.0034 V

As can be seen in Table 5, the statistical results demonstrate the high accuracy of the Luenberger observer proposed for different databases. Besides, the observer showed high performance in estimating the electrolyzer voltage under continuous changes in input currents, which demonstrates its robustness. This high precision was achieved using values of L in the calculated stability region, $l_1, l_2 > 0$. Therefore, by using this observer it is possible to appreciate the dynamics of the voltage states $v_{\rm act,c}$ and $v_{\rm act,a}$ that occur at the cathode and the anode through an ECM. However, the assumption for $v_{\rm ini}$, $R_{\rm mem}$, and $C_{\rm c} = C_{\rm a}$ (i.e., these parameters are considered constant to facilitate the development of the Luenberger observer) affects the accuracy of measurements for the dynamic voltage $v_{\rm act}$ presented in a real PEM electrolyzer.

V. CONCLUSION

In this work, the effectiveness and robustness of the Luenberger observer were demonstrated for the dynamics present in the PEM electrolyzer voltage when subjected to continuous changes in input currents.

The effectiveness of the implementation of the Luenberger observer to an ECM for PEM electrolyzer voltage opens new research opportunities for different implementations of observers and control. Furthermore, by using the ECM parameters and implementing the Luenberger observer it is possible to build an electronic circuit that emulates the real voltage response of a PEM electrolyzer in a reliable way and that also allows for estimating dynamic behaviors.

ACKNOWLEDGMENT

The authors are grateful to Dr. Isaac Zetina and Dr. Dulce Serrano for their support in the observer study and Dr. Bahia Cassal for her support in the development of the Luenberger observer code.

REFERENCES

[1] L. M. Abadie and J. M. Chamorro, "Investment in wind-based hydrogen production under economic and physical uncertainties," *Appl. Energy*, vol. 337, May 2023, Art. no. 120881.

[2] *Net Zero by 2050*, Int. Energy Agency, Paris, France, 2021. [Online]. Available: https://www.iea.org/reports/net-zero-by-2050

[3] E. Escobedo, D. García, M. Ruiz, A. Izquierdo, D. Pacheco-Catalán, and L. C. Ordóñez, "Design, construction, and performance of a próton exchange membrane water electrolyzer (PEM-WE)," *Int. J. Electrochem. Sci.*, vol. 18, no. 5, May 2023, Art. no. 100110.

[4] F. Gutiérrez-Martín, L. Amodio, and M. Pagano, "Hydrogen production by water electrolysis and off-grid solar PV," *Int. J. Hydrogen Energy*, pp. 29038–29048, Oct. 2020.

[5] M. Kheirrouz, F. Melino, and M. A. Ancona, "Fault detection and diagnosis methods for green hydrogen production: A review," *Int. J. Hydrogen Energy*, vol. 47, no. 65, pp. 27747–27774, Jul. 2022.

[6] S. Becker and V. Karri, "Predictive models for PEM-electrolyzer performance using adaptive neuro-fuzzy inference systems," *Int. J. Hydrogen Energy*, vol. 35, no. 18, pp. 9963–9972, Sep. 2010.

[7] M. E. Günay and N. A. Tapan, "Analysis of PEM and AEM electrolysis by neural network pattern recognition, association rule mining and LIME," *Energy AI*, vol. 13, Jul. 2023, Art. no. 100254.

[8] X. Lu, B. Du, S. Zhou, W. Zhu, Y. Li, Y. Yang, C. Xie, B. Zhao, L. Zhang, J. Song, and Z. Deng, "Optimization of power allocation for wind-hydrogen system multi-stack PEM water electrolyzer considering degradation conditions," *Int. J. Hydrogen Energy*, vol. 48, no. 15, pp. 5850–5872, Feb. 2023.

[9] J. Koponen, A. Kosonen, V. Ruuskanen, K. Huoman, M. Niemelä, and J. Ahola, "Control and energy efficiency of PEM water electrolyzers in renewable energy systems," *Int. J. Hydrogen Energy*, vol. 42, no. 50, pp. 29648–29660, Dec. 2017.

[10] L. Järvinen, P. Puranen, A. Kosonen, V. Ruuskanen, J. Ahola, P. Kauranen, and M. Hehemann, "Automized parametrization of PEM and alkaline water electrolyzer polarisation curves," *Int. J. Hydrogen Energy*, vol. 47, no. 75, pp. 31985–32003, Sep. 2022.

[11] A. Majumdar, M. Haas, I. Elliot, and S. Nazari, "Control and control-oriented modeling of PEM water electrolyzers: A review," *Int. J. Hydrogen Energy*, vol. 48, no. 79, pp. 30621–30641, Sep. 2023.

[12] V. A. M. Lopez, H. Ziar, J. W. Haverkort, M. Zeman, and O. Isabella, "Dynamic operation of water electrolyzers: A review for applications in photovoltaic systems integration," *Renew. Sustain. Energy Rev.*, vol. 182, Aug. 2023, Art. no. 113407.

[13] O. Ulleberg, "Modeling of advanced alkaline electrolyzers: A system simulation approach," *Int. J. Hydrogen Energy*, vol. 28, no. 1, pp. 21–33, Jan. 2003.

[14] O. Atlam and M. Kolhe, "Equivalent electrical model for a proton exchange membrane (PEM) electrolyser," *Energy Convers. Manage.*, vol. 52, nos. 8–9, pp. 2952–2957, Aug. 2011.

[15] C. Rozain and P. Millet, "Electrochemical characterization of polymer electrolyte membrane water electrolysis cells," *Electrochimica Acta*, vol. 131, pp. 160–167, Jun. 2014.

[16] D. Guilbert and G. Vitale, "Dynamic emulation of a PEM electrolyzer by time constant based exponential model," *Energies*, vol. 12, no. 4, p. 750, Feb. 2019.

[17] D. Guilbert, D. Sorbera, and G. Vitale, "A stacked interleaved DC–DC buck converter for proton exchange membrane electrolyzer applications: Design and experimental validation," *Int. J. Hydrogen Energy*, vol. 45, no. 1, pp. 64–79, Jan. 2020.

[18] A. Khan, W. Xie, B. Zhang, and L.-W. Liu, "A survey of interval observers design methods and implementation for uncertain systems," *J. Franklin Inst.*, vol. 358, no. 6, pp. 3077–3126, Apr. 2021.

[19] Q. Li, L. Yin, H. Yang, T. Wang, Y. Qiu, and W. Chen, "Multiobjective optimization and data-driven constraint adaptive predictive control for efficient and stable operation of PEMFC system," *IEEE Trans. Ind. Electron.*, vol. 68, no. 12, pp. 12418–12429, Dec. 2021.

[20] Q. Li, P. Liu, X. Meng, G. Zhang, Y. Ai, and W. Chen, "Model prediction control-based energy management combining self-trending prediction and subset-searching algorithm for hydrogen electric multiple unit train," *IEEE Trans. Transport. Electrific.*, vol. 8, no. 2, pp. 2249–2260, Jun. 2022.

[21] T. Puleston, A. Cecilia, R. Costa-Castelló, and M. Serra, "Nonlinear observer for online concentration estimation in vanadium flow batteries based on half-cell voltage measurements," *Comput. Chem. Eng.*, vol. 185, Jun. 2024, Art. no. 108664.

[22] G. E. M. Abro, S. A. B. M. Zulkifli, and V. S. Asirvadam, "Dual-loop single dimension fuzzy-based sliding mode control design for robust tracking of an underactuated quadrotor craft," *Asian J. Control*, vol. 25, no. 1, pp. 144–169, Jan. 2023.

[23] G. E. M. Abro, Z. A. Ali, S. A. Zulkifli, and V. S. Asirvadam, "Performance evaluation of different control methods for an underactuated quadrotor unmanned aerial vehicle (QUAV) with position estimator and disturbance observer," *Math. Problems Eng.*, vol. 2021, pp. 1–22, Dec. 2021.

[24] K. Jing and C. Liu, "Online observer of the voltage components of the PEM electrolyzer based on the time-varying linearization of the semi-empirical model," *Energy Rep.*, vol. 9, pp. 299–307, Sep. 2023.

[25] J. Luna, E. Usai, A. Husar, and M. Serra, "Enhancing the efficiency and lifetime of a proton exchange membrane fuel cell using nonlinear model-predictive control with nonlinear observation," *IEEE Trans. Ind. Electron.*, vol. 64, no. 8, pp. 6649–6659, Aug. 2017.

[26] J. Liu, Y. Gao, X. Su, M. Wack, and L. Wu, "Disturbance-observer-based control for air management of PEM fuel cell systems via sliding mode technique," *IEEE Trans. Control Syst. Technol.*, vol. 27, no. 3, pp. 1129–1138, May 2019.

[27] K. E. K. Benkara, A. Alchami, A. N. Eddine, G. Bakaraki, and C. Forgez, "Field programmable gate arrays implementation of a Kalman filter based state of charge observer of a lithium ion battery pack," *J. Energy Storage*, vol. 70, Oct. 2023, Art. no. 107860.

[28] Y. Xu, X. Ge, and W. Shen, "Multi-objective nonlinear observer design for multi-fault detection of lithium-ion battery in electric vehicles," *Appl. Energy*, vol. 362, May 2024, Art. no. 122989.

[29] Y. Su, Z. Shi, and T. Wachtler, "A Bayesian observer model reveals a prior for natural daylights in hue perception," *Vis. Res.*, vol. 220, Jul. 2024, Art. no. 108406.

[30] P. Wang, H. Wang, X. Cai, and Z. Han, "Flux detection by using impulsive observer for wind energy application," *J. Circuits, Syst. Comput.*, vol. 22, no. 7, Aug. 2013, Art. no. 1350054.

[31] Z.-T. Xie, B. Liu, Y.-Z. Liu, and Z. Sun, "Event-triggered impulsive observer with K-asymptotic gain for DC microgrids," *Int. J. Electr. Power Energy Syst.*, vol. 156, Feb. 2024, Art. no. 109752.

[32] F. C. Rego, Y. Pu, A. Alessandretti, A. P. Aguiar, A. M. Pascoal, and C. N. Jones, "A distributed Luenberger observer for linear state feedback systems with quantized and rate-limited communications," *IEEE Trans. Autom. Control*, vol. 66, no. 9, pp. 3922–3937, Sep. 2021.

[33] J. M. Ali, N. H. Hoang, M. A. Hussain, and D. Dochain, "Review and classification of recent observers applied in chemical process systems," *Comput. Chem. Eng.*, vol. 76, pp. 27–41, May 2015.

[34] I. Dincer and A. A. AlZahrani, "4.25 electrolyzers," in *Comprehensive Energy Systems*. Oxford, U.K.: Elsevier, 2018, pp. 985–1025.

[35] D. S. Falcão and A. M. F. R. Pinto, "A review on PEM electrolyzer modelling: Guidelines for beginners," *J. Cleaner Prod.*, vol. 261, Jul. 2020, Art. no. 121184.

[36] S. Mucci, A. Mitsos, and D. Bongartz, "Power-to-X processes based on PEM water electrolyzers: A review of process integration and flexible operation," *Comput. Chem. Eng.*, vol. 175, Jul. 2023, Art. no. 108260.

[37] M. Langemann, D. L. Fritz, M. Müller, and D. Stolten, "Validation and characterization of suitable materials for bipolar plates in PEM water electrolysis," *Int. J. Hydrogen Energy*, vol. 40, no. 35, pp. 11385–11391, Sep. 2015.

[38] Á. Hernández-Gómez, V. Ramirez, D. Guilbert, and B. Saldivar, "Development of an adaptive static-dynamic electrical model based on input electrical energy for PEM water electrolysis," *Int. J. Hydrogen Energy*, vol. 45, no. 38, pp. 18817–18830, Jul. 2020.

[39] Á. Hernández-Gómez, V. Ramirez, D. Guilbert, and B. Saldivar, "Cell voltage static-dynamic modeling of a PEM electrolyzer based on adaptive parameters: Development and experimental validation," *Renew. Energy*, vol. 163, pp. 1508–1522, Jan. 2021.

[40] H. Gorgun, ''Dynamic modelling of a proton exchange membrane (PEM) electrolyzer,'' *Int. J. Hydrogen Energy*, vol. 31, no. 1, pp. 29–38, Jan. 2006.
[41] R. García-Valverde, N. Espinosa, and A. Urbina, ''Simple PEM water electrolyser model and experimental validation,'' *Int. J. Hydrogen Energy*, vol. 37, no. 2, pp. 1927–1938, Jan. 2012.
[42] T. Kailath, *Linear Systems*, vol. 156. Englewood Cliffs, NJ, USA: Prentice-Hall, 1980.
[43] K. Ogata, *Ingenieria De Control Moderna*, vol. 5. Upper Saddle River, NJ, USA: Prentice-Hall, 2010.

ÁNGEL HERNÁNDEZ-GÓMEZ received the Ph.D. degree in science from the Yucatan Scientific Research Center (CICY), Yucatán, Mexico, in 2022. He is currently a Postdoctoral Researcher with the School of Sciences, Universidad Autónoma de San Luis Potosí (UASLP), San Luis Potosí, Mexico. His current research interests include dynamic systems, control theory, and PEMFC and PEM electrolyzer modeling.

DIEGO LANGARICA-CORDOBA (Senior Member, IEEE) received the Ph.D. degree in engineering from the Universite de Paris Sud XI, Orsay, France, in 2014. He is currently a Researcher with the School of Sciences, Universidad Autónoma de San Luis Potosí (UASLP), San Luis Potosí, Mexico. His current research interests include nonlinear control theory, power conversion, renewable energy, and electric vehicles.

PANFILO R. MARTINEZ-RODRIGUEZ (Senior Member, IEEE) received the Ph.D. degree in applied science from the Instituto Potosino de Investigacion Cientifica y Tecnologica A.C. IPICYT, San Luis Potosí, Mexico, in 2007. From 2006 to 2016, he was a full-time Professor with the Tecnologico de Mexico, Instituto Tecnologico Superior de Irapuato, TecNM-ITESI, Mexico. Since 2017, he has been a Professor-Researcher with the Facultad de Ciencias, Universidad Autónoma de San Luis Potosí, Mexico. His research interests include power electronics applications; the modeling, design, and control of power electronics converters applied to the improvement of the electrical power quality; and the electrical energy conversion from non-conventional electrical power sources.

HERNÁN GONZÁLEZ-AGUILAR received the Ph.D. degree in sciences (mathematics) from the Center for Research in Mathematics (CIMAT), Guanajuato, México, in 2007. He is currently a Researcher with the School of Sciences, Universidad Autónoma de San Luis Potosí (UASLP). His current research interests include discrete and computational geometry, dynamic systems, and applied mathematics.

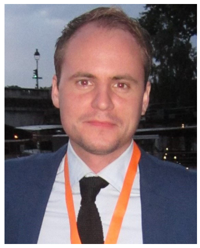

DAMIEN GUILBERT (Member, IEEE) was born in Paris, France, in 1987. He received the M.Sc. degree in electrical engineering and control systems and the Ph.D. degree in electrical engineering from the University of Technology of Belfort-Montbliard, Belfort, France, in 2011 and 2014, respectively, and the Habilitation à Diriger des Recherches degree in electrical engineering from the University of Lorraine, Longwy, France, in 2022. From 2016 to 2023, he was an Associate Professor with the University of Lorraine, France; and a permanent member of the Group of Research in Electrical Engineering of Nancy (GREEN) Laboratory. Since 2023, he has been a Full Professor with the University of Le Havre Normandy, Le Havre, France; and has been a permanent member of the Group of Research in Electrical Engineering and Automatic Control of Le Havre (GREAH). His current research interests include power electronics for electrolyzer applications, electrolyzer modeling and emulation, and energy management of multisource systems relying on renewable energy sources and hydrogen technologies.

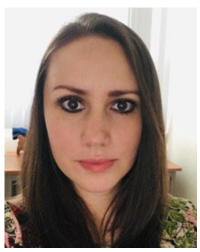

BELEM SALDIVAR received the B.S. degree in electronics and telecommunications engineering from the Autonomous University of Hidalgo State, UAEH, Mexico, in 2007, the M.Sc. degree in automatic control from the Center for Research and Advanced Studies, National Polytechnic Institute CINVESTAV, Mexico City, Mexico, in 2010, and the dual Ph.D. degree in automatic control from CINVESTAV and in informatics and its applications from the Research Institute of Communication and Cybernetics of Nantes, IRCCyN, Nantes, France, in 2013. From 2014 to 2022, she was a Research Professor of the Catedras CONACyT Program, Faculty of Engineering, Autonomous University of the State of Mexico. Since 2022, she has been a full-time Professor with the Department of Automatic Control, CINVESTAV-IPN, Mexico. Her research is focused on modeling and control of (finite and infinite-dimensional) dynamic systems and nonlinear and time delay systems.